Dielectric behaviour of non-spherical cell suspensions

2001 J. Phys.: Condens. Matter 13 3583

(http://iopscience.iop.org/0953-8984/13/15/302)

INSTITUTE OF PHYSICS PUBLISHING JOURNAL OF PHYSICS: CONDENSED MATTER

J. Phys.: Condens. Matter **13** (2001) 3583–3589 www.iop.org/Journals/cm PII: S0953-8984(01)20979-5

Dielectric behaviour of non-spherical cell suspensions

Jun Lei[1,2], Jones T K Wan[1], K W Yu[1] and Hong Sun[2,3]

[1] Department of Physics, Chinese University of Hong Kong, Shatin, NT, Hong Kong
[2] Department of Applied Physics, Shanghai Jiao Tong University, Shanghai 200 030, China
[3] Department of Physics, University of California, Berkeley, California 94720-7300, USA

Received 16 January 2001, in final form 6 March 2001

Abstract

Recent experiments revealed that the dielectric dispersion spectrum of fission yeast cells in a suspension was mainly composed of two sub-dispersions. The low-frequency sub-dispersion depended on the cell length, whereas the high-frequency one was independent of it. The cell shape effect was qualitatively simulated by an ellipsoidal-cell model. However, the comparison between theory and experiment was far from being satisfactory. In an attempt to close up the gap between theory and experiment, we considered the more realistic cells of spherocylinders, i.e. circular cylinders with two hemispherical caps at both ends. We have formulated a Green function formalism for calculating the spectral representation of cells of finite length. The Green function can be reduced because of the azimuthal symmetry of the cell. This simplification enables us to calculate the dispersion spectrum and hence assess the effect of cell structure on the dielectric behaviour of cell suspensions.

1. Introduction

Dielectric spectroscopy has become a quantitative method of real-time monitoring of cell growth in suspensions [1–3]. The real-time monitoring has advantages over conventional techniques and would be important to investigate the dynamic behaviour of cell growth. There are many factors that may influence the dielectric behaviour of biological materials: structure, orientation of dipoles, surface conductances, membrane transport processes, etc. All these factors influence one another and it is difficult to separate out the effect of a single one. However, some effects can be dominant at certain ranges of frequencies. For instance, the dielectric dispersion spectrum of living cell suspensions in radiofrequencies is mainly determined by the cell shape. The objective of this work is to develop a theory for such correlation, on which new applications in biotechnology rely.

More recently, Asami [4] reported that the dielectric dispersion spectrum of fission yeast cells in a suspension was mainly composed of two sub-dispersions. The experimental data revealed that the low-frequency sub-dispersion depended on the cell length, while the high-frequency one was independent of it. Asami adopted a shell-ellipsoid model [3], in which an ellipsoid is covered with an insulating shell as the electrical model of non-spherical biological cells. The comparison between model calculation [3] and experimental data [4] was far from

being satisfactory. Asami suggested that the discrepancy is attributed to the rod-like cell shape. However, the depolarization factor needed in his theory is difficult to calculate for cells of rod-like shape because of a lack of available theories.

In this work, we propose the use of the spectral representation [5] for analysing the cell models. The spectral representation is a rigorous mathematical formalism of the effective dielectric constant of a two-phase composite material [5]. It offers the advantage of the separation of material parameters (namely the dielectric constant and conductivity) from the cell structure information, thus simplifying the study. From the spectral representation, one can readily derive the dielectric dispersion spectrum, with the dispersion strength as well as the characteristic frequency being explicitly expressed in terms of the structure parameters and the materials parameters of the cell suspension (see section 3 below). The actual shape of the real and imaginary parts of the permittivity over the relaxation region can be uniquely determined by the Debye relaxation spectrum, parametrized by the characteristic frequencies and the dispersion strengths. So, we can study the impact of these parameters on the dispersion spectrum directly.

2. Formalism

2.1. Spectral representation theory

We consider a two-component composite dielectric with complex dielectric constant $\epsilon(\boldsymbol{r})$ equal to $\epsilon_2 = \varepsilon_2 + \sigma_2/j2\pi f$ in the host medium and $\epsilon_1 = \varepsilon_1 + \sigma_1/j2\pi f$ in the embedding medium. An interface Σ separates the two media. In a uniform applied electric field $E_0\hat{\boldsymbol{z}}$ (for convenience, let $E_0 = -1$), the electrostatic potential satisfies the Laplace's equation:

$$\nabla \cdot \left[\left(1 - \frac{1}{s}\eta(\boldsymbol{r}) \right) \nabla \Phi(\boldsymbol{r}) \right] = 0 \tag{1}$$

where $s = \epsilon_2/(\epsilon_2 - \epsilon_1)$ denotes the relevant material parameter and $\eta(\boldsymbol{r})$ is the characteristic function of the composite, having value 1 for $\boldsymbol{r}$ in the embedding medium and 0 otherwise. The electric potential $\Phi(\boldsymbol{r})$ can be solved formally as:

$$\Phi(\boldsymbol{r}) = \Phi_0(\boldsymbol{r}) + \frac{1}{s}\int \mathrm{d}\boldsymbol{r}'\eta(\boldsymbol{r}')\nabla' G_0(\boldsymbol{r} - \boldsymbol{r}') \cdot \nabla' \Phi(\boldsymbol{r}') \tag{2}$$

where $G_0(\boldsymbol{r} - \boldsymbol{r}') = 1/4\pi|\boldsymbol{r} - \boldsymbol{r}'|$ is the free-space Green function, and $\Phi_0(\boldsymbol{r}) = \boldsymbol{r} \cdot \hat{\boldsymbol{z}}$ is the potential of the unperturbed uniform field E_0. It is instructive to convert the volume integration into the surface integration via the Green second identity and only deal with the potential on the interface Σ [6]. We denote an integral-differential operator Γ:

$$\Gamma\Phi(\boldsymbol{r}) = \oint_{\Sigma}' \mathrm{d}\boldsymbol{s}' \cdot \nabla' G_0(\boldsymbol{r} - \boldsymbol{r}')\Phi(\boldsymbol{r}') + \tfrac{1}{2}\Phi(\boldsymbol{r}) \qquad \boldsymbol{r} \in \Sigma \tag{3}$$

to avoid the singularity of $G_0(\boldsymbol{r} - \boldsymbol{r}')$ when the integration variable $\boldsymbol{r}'$ approaches the point of $\boldsymbol{r}$ [6]. The integration with a 'prime' denotes the restricted integration which excludes $\boldsymbol{r}' = \boldsymbol{r}$. Let $\Psi_n(\boldsymbol{r})$ and s_n be the nth eigenfunction and eigenvalue of the Γ operator respectively. We can expand $\Phi_0(\boldsymbol{r})$ and $\Phi(\boldsymbol{r})$ on the interface Σ in a series expansion of eigenfunction $\Psi_n(\boldsymbol{r})$:

$$\Phi_0(\boldsymbol{r}) = \sum_n z_n \Psi_n(\boldsymbol{r}) \tag{4}$$

$$\Phi(\boldsymbol{r}) = \sum_n \frac{s z_n}{s - s_n}\Psi_n(\boldsymbol{r}) \tag{5}$$

where z_n are the expansion coefficients. Then we can write the effective dielectric constant $\bar{\epsilon}$ in the Bergman–Milton representation [5]:

$$\bar{\epsilon} = -\frac{1}{V}\int \mathrm{d}V\epsilon(\boldsymbol{r})E_z \tag{6}$$

$$= \frac{1}{V}\int \mathrm{d}V\epsilon_0\left[1-\frac{1}{s}\eta(\boldsymbol{r})\right]\frac{\partial\Phi}{\partial z} \tag{7}$$

$$= \epsilon_0\left[1-\frac{1}{V}\sum_n \frac{z_n}{s-s_n}\oint_\Sigma \mathrm{d}\boldsymbol{s}\cdot\hat{z}\Phi_n(\boldsymbol{r})\right] \tag{8}$$

$$= \epsilon_0\left[1-p\sum_n \frac{f_n}{s-s_n}\right] \tag{9}$$

where p is the volume fraction of the suspending cells. Note that E_z is a dimensionless electric field because $E_0 = -1$. The eigenvalue s_n and the spectral function f_n can be proved to be real and satisfy simple properties that $0 < s_n < 1$, $f_n > 0$ and $\sum f_n = 1$. We shall show that both the spectral function f_n and the eigenvalue s_n determine the dielectric behaviour of cell suspensions.

2.2. Cells with an axis of revolution

Now the principal problem is to calculate the eigenvalue s_n and the spectral function f_n. For many cells interacting with one another, it is a formidable task. However, in the limit of a dilute cell suspension and weak applied field, one can regard the cells in suspension as being non-interacting and randomly oriented and the problem is reduced to that of a single cell. We will consider cells with an axis of revolution, namely, the spheroidal and the spherocylinder cells [7] to mimic cells of rod-like shape. The prolate spheroid is generated by rotating an ellipse around its major axis, while the spherocylinder is obtained by fitting two hemispherical caps at both ends of a circular cylinder. For a prolate spheroid, the eigenvalues and eigenfunctions can be calculated exactly. The only non-zero f_n equals unity for E_0 being along the major or minor axis of the prolate spheroid, and the corresponding eigenvalues are given by:

$$s_z = -\frac{1}{q^2-1} + \frac{q\ln\left[q+(q^2-1)^{1/2}\right]}{\left(q^2-1\right)^{3/2}} \tag{10}$$

$$s_x = (1-s_z)/2 \tag{11}$$

where z and x refer to the direction along the major and minor axis respectively. For a spherocylinder, the consideration of the symmetry properties of the cell will help us choose the appropriate orthogonal basis for calculating the matrix elements of the Γ operator. Because of the rotation symmetry about the major axis of the spherocylinder, the eigenfunction is necessarily of the form $(a_n\cos n\theta + b_n\sin n\theta)f(x)$ with n being an integer. Due to the inversion symmetry of the cell, $f(x)$ must be either odd or even functions. It is convenient to expand $f(x)$ in a series of Legendre polynomials $P_m(x/l)$, where $2l$ is the length of the cell. The applied uniform field E_0 can always be resolved into two components along the major and minor axes of the spherocylinder, so we can calculate the s_n and f_n for E_0 along the major and minor axes separately. By symmetry, in order to obtain a non-zero f_n, the eigenfunction should be the form of $\sum A_m P_{2m+1}(x/l)$ for E_0 being along the major axis, while it reads $\cos\theta\sum B_m P_{2m}(x/l)$ for E_0 being along the minor axis, with $m = 0, 1, 2, \ldots$. Using this orthogonal basis, we can calculate a truncated matrix according to the precision needed. We should remark that the matrix is generally non-symmetric.

3. Dielectric dispersion spectrum

We show here that from the spectral representation, one can readily derive the dielectric dispersion spectrum. Substituting $\epsilon_1 = \varepsilon_1 + \sigma_1/j2\pi f$ and $\epsilon_2 = \varepsilon_2 + \sigma_2/j2\pi f$ (ε and σ being the real and imaginary parts of the complex dielectric constant) into equation (9), defining a new parameter $t = \sigma_2/(\sigma_2 - \sigma_1)$ and re-defining $s = \varepsilon_2/(\varepsilon_2 - \varepsilon_1)$, we rewrite the effective dielectric constant $\overline{\epsilon}$ after simple manipulations:

$$\overline{\epsilon} = \epsilon_H + \sum_n \frac{\Delta\epsilon_n}{1 + jf/f_n^c} + \frac{\sigma_L}{j2\pi f} \tag{12}$$

where ϵ_H and σ_L are the high-frequency dielectric constant and the low-frequency conductivity respectively, while $\Delta\epsilon_n$ are the dispersion magnitudes, f_n^c are the characteristic frequencies of the nth sub-dispersion.

We have already shown that there are only two poles in the spectral representation of the prolate spheroids. In the following, we will show that there are two dominant poles in the spectral representation of the spherocylinder and hence there are two sub-dispersions in the dielectric dispersion spectrum. The dispersion magnitudes and dispersion frequencies are given by:

$$\Delta\epsilon_1 = \frac{1}{3} p\varepsilon_2 \frac{s_1(s-t)^2}{s(s-s_1)(t-s_1)^2} \tag{13}$$

$$\Delta\epsilon_2 = \frac{2}{3} p\varepsilon_2 \frac{s_2(t-s)^2}{s(s-s_2)(t-s_2)^2} \tag{14}$$

$$f_1^c = \frac{\sigma_2 s(t-s_1)}{2\pi\varepsilon_2 t(s-s_1)} \tag{15}$$

$$f_2^c = \frac{\sigma_2 s(t-s_2)}{2\pi\varepsilon_2 t(s-s_2)}. \tag{16}$$

Thus, we are able to obtain the dispersion strengths as well as the characteristic frequencies explicitly in terms of the structure parameters and the materials parameters of the cell suspension.

The dielectric dispersion spectrum of a dilute suspension of prolate spheroids is mainly composed of two sub-dispersions, namely, s_z is responsible for the lower frequency one and s_x for the higher one. For a spherocylinder, we obtain a non-vanishing series of f_n and s_n. Along the major axis, f_1 is dominant for all q and we can omit the smaller ones. This dominant f_1 is plotted in figure 1 against q, and the corresponding s_z are plotted in figure 2, together with the exact result of a prolate spheroid. As is evident in figure 2, we can see that the difference between the two models is indeed small. Along the minor axis, the solution becomes more complicated. The dominant f_2 near $q = 1$ decreases quickly as q increases; another f_3 increases and takes over at large q. These two f_n are also plotted in figure 1 and their corresponding eigenvalues are plotted in figure 3. As shown in figure 3, the two eigenvalues tend to that of a prolate spheroid in the limit of both small and large q.

Near $q = 2$, the two f_n have comparable values, resulting in two sub-dispersions at higher frequency. These sub-dispersions can interfere with each other, rendering it difficult to find the characteristic frequencies of the different sub-dispersions. Physically, the local field is the most non-uniform in this case. Nevertheless, we will consider cells of large length and omit this complication.

With equations (13)–(16), it is easy to calculate the effect of the rod-like cell structure on the dispersion spectrum and to compare with experiment data. We will show that the spherocylinder model does give some improvement towards the experimental result.

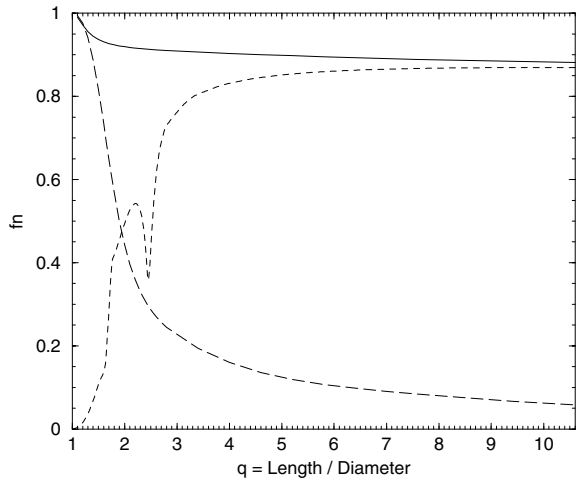

Figure 1. The three dominant f_n plotted against the axial ratio q: f_1 along the major axis (solid line), f_1 along the minor axis (long dashed line) and f_2 along the minor axis (short dashed line).

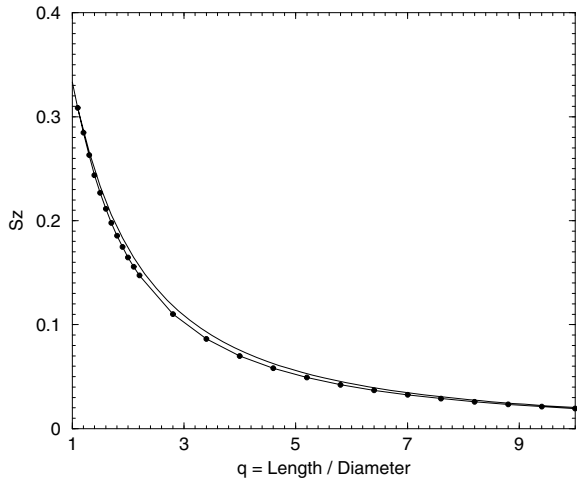

Figure 2. The eigenvalue s_n associated with f_n along the major axis plotted against the axial ratio q: the spherocylinder cell (solid line with filled circles), and the exact result of the prolate spheroid (solid line).

However, the improvement is too small to close up the gap as Asami expected. In fact, we shall see that Asami omitted the material parameters which will play an important role in the experimental condition. By introducing the conductivity contrast $t = \sigma_2/(\sigma_2 - \sigma_1)$, we found that a small negative t, i.e. $\sigma_1 \gg \sigma_2$, should be used to close up the discrepancy.

We estimate t and s by fitting equations (13)–(16) to the experimental ratio of $\Delta\epsilon_1/\Delta\epsilon_2$ and f_2^c/f_1^c, and we get $t = -0.0014$ and $s = 5.0$. It means that $\sigma_1 \approx 700\sigma_2$ and $\varepsilon_1 \approx 0.80\varepsilon_2$. The enhanced conductivity of cell cytoplasm is attributed to the membrane potential. The result is in contrast to the previous (unjustified) claim that $\sigma_1 \approx \sigma_2$.

Table 1 lists the $\Delta\epsilon_1/\Delta\epsilon_2$ ratio and f_2^c/f_1^c ratio for both experimental and theoretical results. Using the fitting material parameters, the improvement is obvious for both the

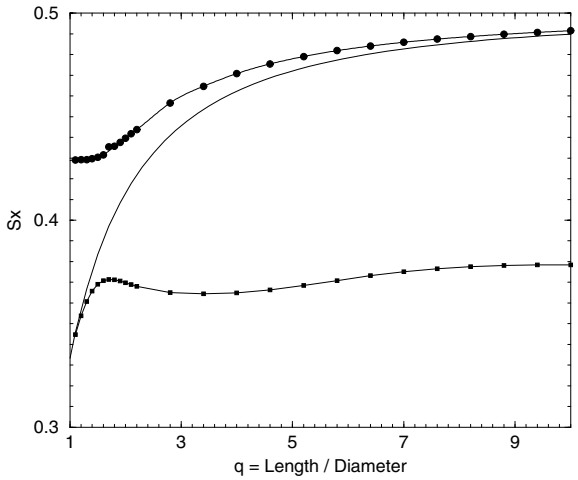

Figure 3. The eigenvalue s_n associated with f_n along the minor axis plotted against the axial ratio q: s_1 of the spherocylinder cell (solid line with filled squares), s_2 of the spherocylinder cell (solid line with filled circles), and the exact result of the prolate spheroid (solid line).

Table 1. The ratios of the characteristic frequencies $\Delta\epsilon_1/\Delta\epsilon_2$ and the ratios of the dispersion strengths f_2^c/f_1^c listed as a function of the length to diameter ratio q of the cells. The experimental results were extracted from [4] together with the theoretical predictions. Both the prolate-spheroid model and the spherocylinder model adopt the same fitting material parameters determined from the experimental data.

	Experimental result		Asami theory		Prolate-spheroid model		Spherocylinder model	
q	$\Delta\epsilon_1/\Delta\epsilon_2$	f_2^c/f_1^c	$\Delta\epsilon_1/\Delta\epsilon_2$	f_2^c/f_1^c	$\Delta\epsilon_1/\Delta\epsilon_2$	f_2^c/f_1^c	$\Delta\epsilon_1/\Delta\epsilon_2$	f_2^c/f_1^c
3.46	2.22	8.95	0.900	3.00	2.26	5.34	2.77	5.89
7.17	8.65	27.4	2.07	7.73	6.10	15.3	6.67	16.4
10.2	16.4	52.6	3.39	13.0	9.94	25.9	10.5	27.2

prolate-spheroid model and the spherocylinder model, while the difference between the two models is quite small.

Discussion and conclusion

In this work, we have applied the spectral representation to the dielectric dispersion of suspensions of fission yeast cells. As mentioned by Asami [4], the discrepancies between theory and experiment may be attributed to the rod-like cell shape. For cells of non-conventional shape, however, there exists no available cell model in the literature and we must develop the spectral representation from first principles.

More precisely, we have developed a Green function formalism [6,8] for calculating the spectral representation of rods of finite length. We modelled the rod-like cells as the spherocylinders, i.e. circular cylinders with two hemispherical caps at both ends. We solved the spectral representation of the effective dielectric constant from first principles. Similar formalism was adopted for cell suspensions near their sub-division point [9–11].

Generally speaking, when the axial ratio q is larger than 4, the prolate-spheroid model can be employed as a good approximation for rod-like cell structures. For $q < 4$, the dielectric

behaviour will become more sensitive to the cell structure of the suspending particles, and there are more sub-dispersions than that of the prolate spheroid suspensions.

Our model does not include the rotational or vibrational effects, and our results are expected to be valid only for weak electric fields. Our model also ignores the multi-shell nature of the cells. Usually the multi-shell model is used to explain the high-frequency steps of spherical cell suspensions. Similar conclusions were found in one of our previous paper on multi-shell dielectric spheres in electrorheological (ER) fluids [12] to account for the effects of water coating on the ER effects. In [12], we also showed that the spectral representation can still be used for multi-shell model, albeit with a slight modification.

In Asami's experiment, there exist three sub-dispersions, the highest frequency step (above 10 MHz) is due to the vacuole and cell wall as mentioned by Asami, while the two lower frequency steps are evidently dependent on the cell shape. And the disperson magnitude of the highest frequency step is much smaller than that of the two lower frequency ones. So one expects that the multi-shell model has only a small effect on the lower frequency steps. In fact the multi-shell model was used in Asami's theory, but the discrepancy, as we mentioned in the text, is still large.

The large cytoplasmic conductivity is a key result of our investigation. We believe that the large cytoplasmic conductivity is reasonable because the cells have to maintain a higher ion concentration in their cytoplasm to avoid the shrinkage of cells due to a loss of water across the cell membrane. However, to our knowledge, there exists no direct experimental measurement on the cytoplasmic conductivity. In our work, we propose a convenient and practical means of determining the cytoplasmic conductivity from the dielectric spectroscopy data. This analysis could be important for biotechnology.

Acknowledgments

This work was supported in part by the Direct Grant for Research of the Research Committee and in part by the Research Grants Council of the Hong Kong SAR Government. K W Y acknowledges useful conversations with Professor G Q Gu.

References

[1] For a review, see Gimsa J and Wachner D 1998 *Biophys. J.* **75** 1107
[2] Davies E, Woodward A and Kell D 2000 *Bioelectromagnetics* **21** 23
[3] Asami K, Yonezawa T 1995 *Biochim. Biophys. Acta* **1245** 317
[4] Asami K 1999 *Biochim. Biophys. Acta* **1472** 137
[5] Bergman D J 1978 *Phys. Rep.* **43** 379
[6] Yu K W, Hong Sun and J T K Wan 2000 *Physica* B **279** 78
[7] Knipp P A and Reinecke T L 1992 *Phys. Rev.* B **46** 10 310
[8] Gu G Q and Tao R B 1988 *Phys. Rev.* B **37** 8612
[9] Gheorghiu E 1994 *J. Phys. A: Math. Gen.* **27** 3883
[10] Gheorghiu E and Asami K 1998 *Bioelectrochem. Bioenergetics* **45** 139
[11] Prodan C and Prodan E 1999 *J. Phys. D: Appl. Phys.* **32** 335
[12] Yu K W, J T K Wan, Law M F and Leung K K 1998 *Int. J. Mod. Phys.* C **9** 1447